Proceedings of the XII International Symposium on Dynamic Problems of Mechanics (DINAME 2007),
Varoto, P. S. and Trindade, M. A. (Editors), ABCM, Ilhabela, SP, Brazil, February 26 - March 2, 2007

Direct-active and Semi-active Smart Structure Control Systems for Aeroelastic Applications

Fred Nitzsche[1]

[1] Carleton University, Department of Mechanical and Aerospace Engineering, 1125 Colonel By Drive, Ottawa, Ontario, Canada, K1S 5B5

Abstract: This paper deals with practical examples of implementation Smart Structures technology in problems of Aeroelasticity. The different approaches to actively control aeroelastic phenomena can be classified into two main categories: direct active and semi-active. Direct-active approaches are characterized by large control power and thus have limited application in the field. Semi-active approaches are much less demanding in control power requirements. More effective active systems can be envisioned by the combination of the two approaches in hybrid systems composed of cooperative subsystems with multiple control objectives.

Keywords: experimental aeroelastic control, smart structures, buffeting, rotorcraft noise and vibration control.

INTRODUCTION

Suppressing vibration in mechanical systems in general has been a challenging problem in many applications. There are a number of passive vibration control approaches presently in use to address this problem. These passive approaches typically involve the use of stiffeners, dampers, and isolators. In general, these passive approaches can only provide moderate vibration suppression, are only effective in narrow frequency bands, and often incur significant weight penalties. In contrast, active approaches can be used to significantly suppress vibrations in relatively wider frequency bands due to their controllable nature.

Development of various integrated systems incorporating devices and control schemes capable of performing active vibration suppression has been the focus of a multitude of past and present research. Current active vibration suppression schemes can be classified using two broad categories, including direct-active approaches and semi-active approaches. In direct-active concepts, vibration is controlled using direct, forced action against the vibratory forces. In contrast, semi-active approaches perform vibration suppression using controlled variations of impedance characteristics of dynamic systems.

In the direct-active applications there is a requirement that the actuator must supply large actuation displacements in conjunction with large forces, implicitly implying that large power is necessary. The piezoelectric materials are generally ill suited for this dual performance requirement. In general, such smart material actuators are capable of producing relatively high forces, but possess extremely low stroke capabilities; typically on the order of 50μm. This restricted deformation capability results either in the need for complex displacement amplification mechanisms (a trade-off only achievable by reducing the actuator force capability) or application of extremely high voltage to obtain the required power to effectively suppress vibrations. In fact, the high power requirements of the applications using piezoelectric actuators have hindered practical implementations of these concepts in the aeronautical industry.

In semi-active concepts, the vibration is suppressed by modulating the structural properties of a dynamic system such as stiffness, damping or mass. In these approaches, smart materials can be used to perform such modulations in dynamic impedance to suppress vibrations. In contrast to direct-active approaches, the power requirements are relatively low because the actuator forces are not generated to directly counteract the vibratory forces. In fact, in most devices designed for semi-active control the work done by the actuator forces is independent from the work done by the excitation forces that are the objective of control.

This paper will discuss examples of experimental research of aeroelastic control using both the direct-active and semi-active principles.

DIRECT-ACTIVE SYSTEMS

Most of the recent advancements of smart structure in aeroelastic applications use direct-active approaches relying on piezoceramic-based actuators. Piezoceramic materials have the frequency bandwidth that is required for the active control of aeroelastic systems and can be embedded in a composite lightweight structure. One such development was the F-18 fighter vertical fin Buffeting Loading Alleviation (BLA) system that has been investigated under the Technical Cooperation Program involving the United States, Canada and Australia (Ryall et al, 1999).

Other example following in the same category is the Active Twist Rotor (ATR) program that was developed by NASA and other partners in the United States to reduce vibration in helicopter blades (Wilbur et al, 2002; Shin, Cesnik and Hall, 2005). The trailing-edge flap is another example of direct-active concept under investigation for use in rotorcraft to suppress vibratory hub loads and noise. Contrarily to the former approaches, the latter uses a lumped control method, where actuators are located at a determined location in the structure rather than distributed over its surface. The trailing-edge flap can be designed as a servo flap to generate sufficient rotor blade twist deflections resulting in new aerodynamic loads to counteract the vibratory force of the blade. The open- and closed-loop control of a Mach-scaled rotor model with trailing-edge flaps was investigated in wind tunnel (Straub et al, 2001), and more recently a full-scale model was successfully flown by EUROCOPTER (Jaenker et al, 2006).

The F-18 Vertical Fin Buffeting Load Alleviation (BLA) Project

It is difficult to predict buffet loads during the design stage of an aircraft. One such example is the F/A-18. This twin-tail aircraft is often subjected to high-intensity buffet loads that produce accelerations in excess of 450g at the tip the vertical fin during maneuvers at high angles of attack. An initial approach to minimize the problem included aerodynamic and structural changes such as the introduction of a leading-edge extension (LEX) fence. This fence has been added to the aircraft wing root to reduce buffeting by generating additional vortices that interact with the vertical tail and assure airflow attachment to the surface. However, at very high angles of attack, the vortices generated by the LEX fence break down before reaching the tail, generating an even more turbulent wake. The loads produced substantially contribute to the fatigue of the tail structure, increasing the maintenance costs of the fighter.

This problem is of particular concern for those countries within The Technical Co-operation Program, (TTCP) that include the F/A-18 in their fleets. The TTCP is a program of technical collaboration and data exchange among five nations: Canada, the United States, Australia, United Kingdom and New Zealand. Of these participants, three countries, namely Canada, the United States, and Australia initiated the collaborative research program nicknamed BLA aimed at smart structures solutions to the problem. The overall approach of the program is to develop an active control system that includes strain actuation using piezoelectric elements. However, the ability of the piezoelectric actuators to achieve control authority under the large aerodynamic buffet loads in a full-scaled aircraft needed to be demonstrated. Ground Vibration Tests (GVT) occurred under the TTCP program with the objective of evaluating the performance of the smart structure solution. In this program, Australia contributed the test rig; Canada offered the input data information in the form of representative buffet time sequences measured in flight, and the United States provided the control system hardware. All TTCP partners contributed to the software design with unique control strategies.

The initial closed-loop tests of the proposed active control system were carried out in the International Follow-on Structural Test (IFOST) rig in Melbourne, Australia, in 1998. These tests represented an important milestone on the development of adaptive structures systems with application to aeroelastic problems because they were the first tests performed on a full-scale airframe to achieve aerodynamic buffet alleviation. The objectives of the ground vibration test were: (1) to demonstrate active buffet suppression in a full-scale aircraft; (2) to measure vibration level reductions at different points on the tail, most significantly, at the critical points situated at the fin root where fatigue cracks have been spotted due to high bending stress; (3) to demonstrate piezoelectric control authority at full buffet loads; and (4) to measure vibration reduction at different flight conditions demonstrating the controller robustness under different excitation loads. The next section will summarize the effort of the Canadian team, which main objective was to investigate the most promising combination of sensors to achieve the required performance using the hardware provided by the American team (Nitzsche, Liberatore and Zimcik, 1998). This hardware was configured to accept a Multiple Input Multiple Output (MIMO) feedback control system with two inputs (consisting of a choice among several strain gauges and accelerometers distributed over the surface of the vertical fin to measure the performance of the system), and two outputs that drove two groups of piezoelectric actuators attached to both sides of the structure skin.

Simulation Model

Previous investigations in F-18 vertical tail buffeting were able to demonstrate that the first and the second natural modes of the fin structure contribute most significantly to the buffeting phenomenon (Mode 1, the first bending of the vertical fin at approximately 17Hz and Mode 2, the first torsion of the vertical fin at approximately 45Hz). Therefore, a NASTRAN finite-element detailed model was built to represent as close as possible the dynamics of the structure at the low frequencies of interest. Shell elements were used to model both the skin and the internal stiffeners of the fin. Rod elements were employed to simulate the piezoelectric patches working in unison in a push-pull configuration across the fin structure (out-of-phase extension-compression mode to generate bending). The latter elements were distributed along seven spanwise rows lying on the two skins of the fin, approximating the actual distribution of actuators suggested by the hardware designers to achieve authority over the buffeting phenomenon. In addition, beam elements were defined to connect the parts where the rod elements that represented the actuators were separated to form two independent groups. In principle, these two independent groups of actuators were able to approximately perform Independent Modal State Control (IMSC), improving the realization of a more efficient and robust closed-loop aeroelastic system. Hence, each actuation group had more control authority over one specific mode of the structure (Group 1 to Mode 1 and Group 2 to Mode 2). Since the fin was a composite structure, several isotropic material properties were defined. To complete the aeroelastic model in NASTRAN (using the doublet-lattice method), the lifting

surface was divided into trapezoidal elements (boxes) arranged in strips parallel to the free stream; two panels in the lower and upper parts of the vertical fin were defined. The boxes were concentrated near the leading and trailing edges of the fin, and along the rudder hinge line. Interference elements simulated the aerodynamic interference effects among the bodies and the lifting surfaces, and one additional interference element was defined to simulate the interference effects between the fuselage, nacelle and the vertical fin.

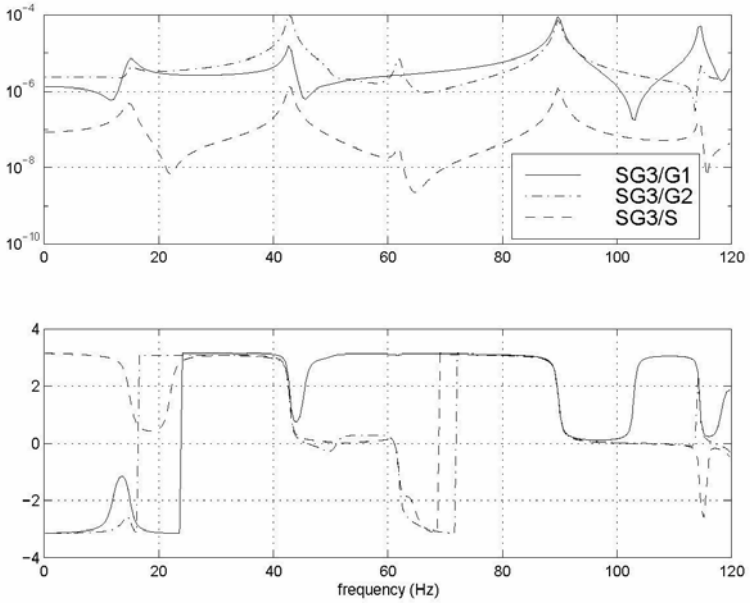

Figure 1 – Transfer functions magnitude and phase plots: Groups 1 and 2 (G1 and G2) and Shaker (S) to Strain Gauge SG3 (vertical fin root) obtained with NASTRAN model.

In order to simulate the piezoelectric strain actuation, the thermal analogy and the aeroelastic frequency response analysis available in NASTRAN were used in a two-step procedure. First, a static and constant temperature field was applied only on the rod elements that represented the piezoelectric actuators. The temperature field had the same magnitude but opposite signs for elements lying on the opposite sides of the fin. The reaction forces at the nodes of the rod elements that represented the piezoelectric actuators were obtained. The thermal loads used in the NASTRAN model were further calibrated to the actual piezoelectric loads obtained in the open-loop system identification tests, when each actuation group was fed with a white noise signal input to reproduce the maximum values of strain when operating alone and at full gain (at saturation voltage). In a second step, the aeroelastic frequency response of NASTRAN was employed to obtain the open-loop transfer functions between the two control inputs (actuation groups), the third input, the disturbance (buffet load), and the two output variables (a choice among four accelerometers and five strain-gauge positions). An example of the 6 transfer functions obtained is depicted in Fig. 1. In order to reproduce the experimental setup better, the disturbance input was applied at a single point of the structure – the shaker position defined in the GVT to simulate the buffeting input load. The Power Spectral Density (PSD) of the disturbance was a known input obtained from the flight tests. Due to hardware limitations, they were band-limited. The frequency content lying outside of each one of the critical modes for buffeting was cut off and the input signal was limited within the bands between 10 and 20Hz for Mode 1 and 35 and 55Hz for Mode 2.

Next, the transfer function data was transferred to MATLAB for control synthesis. A 3×2 MIMO state-space representation of the system was constructed using polynomial fitting of the complex data to achieve an approximation for the 6 transfer functions in the frequency interval of interest. Due to the fact that state-space representations are not unique, the polynomials did not carry a common denominator (whose roots should represent the poles or the aeroelastic modal frequencies of the actual structure at the flight conditions) and an optimization technique was employed to find the "best" fit in the least square sense of all transfer function elements bearing a common denominator. This was found to be an important step to produce a balanced regulator using the Optimal Control Theory, where the buffeting was treated as a disturbance. The typical regulator was designed for performance in the bandwidth defined by 10 and 60Hz, with roll-off at the lower and higher frequencies. The separation theorem of the classic Linear Quadratic Gaussian (LQG) configuration was used to design a Kalman filter estimator and a full-state feedback regulator. Emphasis in the control law synthesis was given to attenuate the dynamic response associated with both the first and second modes of the vertical fin (at 15 and 43Hz). Three 2×2 (two-input, two-output) control laws were designed involving signals from two accelerometers located at the leading and trailing edges of the vertical fin tip and one strain-gauge located at the point at the root where cracks have been identified in the fleet (considered critical regarding the buffeting-induced structural fatigue). These control laws were later updated with experimental data when the open-loop system identification tests were conduced.

Experimental Results

The IFOST rig in Australia was used for the ground vibration tests of the full-scale aircraft. The piezoelectric actuation devices were attached to both sides of the starboard vertical fin. Two banks of amplifies at each side of the fin driving the two groups of actuators acting in opposite phase to generate bending. The amplifiers fed the maximum voltage differential allowed across the piezoelectric devices (approximately 1500Vac peak-to-peak). The third input signal was given by the 5000lbf electromagnetic shaker attached to a single point at center of the starboard side of the fin through a load cell. Representative time sequences associated with buffeting at different flight conditions analyzed were fed into the computer that controlled the shaker. A load cell was placed between the shaker and the structure to monitor the actual dynamic loads transmitted into the structure by the exciting mechanism. Air bags partially inflated were used to simulate the aerodynamic damping provided by the motion-dependent airloads. Four accelerometers and six strain gauge rosettes situated at strategic points of the fin provided the output signals. In the control room, an 8-channel data acquisition system was used to acquire real-time frequency-domain data including transfer functions and auto-spectra. In addition, a 16-channel digital tape recorder was used to record data from all available signals for subsequent off-line analyses. The signal from two channels could be selected for feedback control through a computer driven DSP board. The experimental set-up is shown in Fig. 2 and a picture of the instrumented vertical fin is presented in Fig. 3.

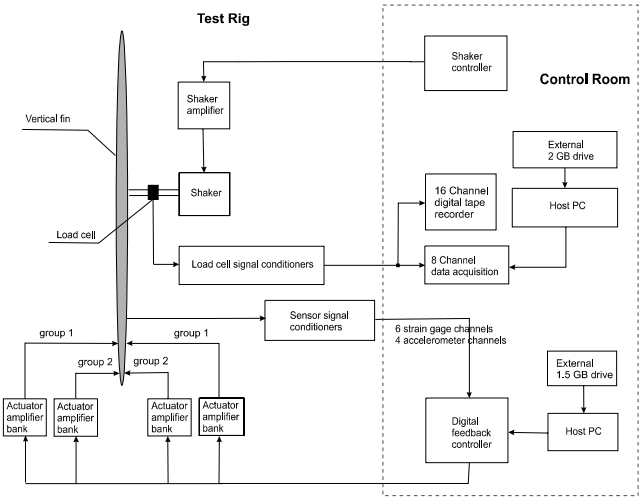

Figure 2 – Ground Vibration Tests experimental setup.

Figure 3 – F-18 instrumented vertical fin.

Very promising results were obtained in the experimental work with a two-input, two-output controller using the linear time invariant LQG design. Vertical fin buffet attenuation exceeding 60% for the nominal flight configuration and 30% for the most severe case was observed during the closed-loop tests. Also, very significant vibration reduction measured by the most important performance metric – the strain gauge located at the critical point for fatigue was verified for the most severe buffeting case: 18% (Mode 2 alone) and 8.7% (Modes 1 and 2 combined). In general, the control laws that included at least one strain gauge in the feedback loop revealed better performance experimentally although all control laws presented similar performance in the numerical simulations using the NASTRAN data. This was an indication that strain gauges were indeed better correlated to the control objective of reducing the structural strain, and that likely the finite-element model did not fully captured the complex characteristics of the composite structure.

In the 1998 tests several actuators failed due to short-circuiting, specially nearest the shaker excitation point, where local stress concentration was observed indicating that the system was still unreliable. Furthermore, the large size and weight of the amplifiers would make the implementation of the active system in the F-18 fleet unpractical. However, the BLA tests were redone in 2005 with improved actuators that presented minimal malfunction and more compact amplifiers, demonstrating that the remarkable progress of the technology in the recent years (Wickramasinghe, Chen and Zimcik, 2006).

SEMI-ACTIVE SYSTEMS

Implementation of semi-active approaches has been performed predominantly using controllable orifice dampers, electrorheological (ER) or magnetorheological (MR) fluids. The capability of MR and ER fluid dampers and variable orifice dampers to achieve significant control of structural damping characteristics has been well established and such devices are fairly readily available. However, somewhat less attention has been given to the development of mechanical devices capable achieving effective control of stiffness characteristics to suppress vibration. It is worthwhile to point out that the possibility of using variations in stiffness to effectively suppress vibrations has been demonstrated in different ways. In particular, it has been shown that controlled variation of the stiffness characteristics associated with dynamic

systems including helicopter rotor blades can result in significant suppression of vibrations (Nitzsche, 2001). Independent study showed that controlled modulation of the stiffness at the root of a helicopter blade could result in significant reduction of vibration energy at target frequencies (Anusonti-Inthra and Gandhi, 2000).

The Smart Spring

It is important to note that most of the semi-active approaches are capable of actively altering a single mechanical property, such as the stiffness or damping or inertia but not the combination of all three properties. In contrast, the Smart Spring is a patented (Nitzsche, Grewal and Zimcik, 1999) adaptive impedance control device that can be designed to preferentially control combinations of the structural stiffness, damping and inertia. It is a unique approach that overcomes several difficulties in other active vibration control approaches.

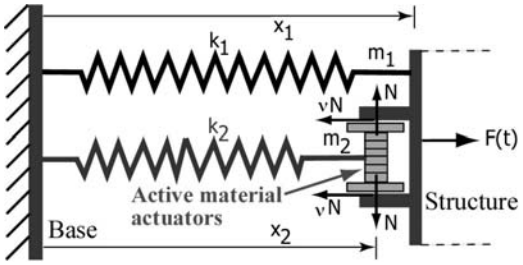

Figure 4 – The Smart Spring semi-active actuator concept.

The mechanism shown in the conceptual drawing in Fig. 4 exploits the large stiffness and bandwidth of the piezoelectric materials to modulate the structural properties to perform active vibration control. It is seen that the device consists of two mass-spring systems. The primary mass-spring system consists of the primary structural mass and stiffness, designated by m_1 and k_1, respectively. In this schematic, the primary structural mass motion is target for control. The secondary, active system consists of the secondary mass and stiffness designated by m_2 and k_2, respectively. The excitation force applied to the primary mass is designated by $F(t)$. The piezoelectric actuators are located on m_2, which is depicted as a plunger, and is attached to the free end of the secondary spring. The plunger, represented by mass m_2 is contained in a sleeve that is integral to the primary mass. The control force is designated by $N(t)$. This control force is generated by the active material actuators and results in the frictional force, $\nu N(t)$. The frictional force acts on the primary and secondary masses in an equal and opposite fashion. It can be seen that the frictional force is the only cause in the depicted system for coupling between the primary and secondary systems. Since the frictional force is directly related to $N(t)$, this coupling is controlled by the actuators.

The purpose of the actuators in the Smart Spring concept is to affect the amount of dynamic coupling between the primary and secondary mass-spring systems. The actuators considered for this application are piezoceramic stacks, which elongate from their neutral length under a positive voltage. In a Smart Spring device, this elongation is practically blocked since the plunger walls in m_2 are in contact with the sleeve that is integral to m_1. This results in a statically indeterminate strain that is shared between the piezoceramic stack and the sleeve. Thus, the control force is a function of the control voltage supplied by the actuators, and the relative stiffness between the actuator and the sleeve structure.

The system in Fig. 4 is a two-degree-of-freedom system consisting of the motion of m_1 and m_2 in the axial direction. It can be also seen that the virtual work done by $N(t)$ is orthogonal to the virtual work done by the external force, $F(t)$. As such, the piezoelectric actuators do not directly perform work against the excitation or the vibratory loads associated with the m_1 motion, which are the objective of control. As previously stated, the Smart Spring concept is a semi-active approach. An interesting property exists in a Smart Spring system and other semi-active systems. Due to the orthogonality between the control and target control forces, no direct transfer function between the control force input and the m_1 displacement output x_1 can be defined (clearly, if m_1 or m_2 are motionless, application of a non-zero input $N(t)$ will not result in a displacement of mass m_1). This is a characteristic of semi-active systems.

Proof-of-concept Hardware

One realization of the Smart Spring concept is depicted in Fig. 5. This prototype was built at the National Research Council of Canada (NRCC) with the objective to control the torsional as opposed to the axial mode of the structure as in the conceptual device depicted in Fig. 4.

As seen in Fig. 5, the off-center shaker simulated the excitation torque from the external disturbance to be controlled by the Smart Spring device. A load transducer installed on the shaker attachment stinger measured the vibratory forces from the shaker. On the opposite side from the shaker a displacement probe measured the vibratory torsional displacement of the "front output plate." The Smart Spring proof-of-concept hardware design shown in Fig. 5 included three actuator units or "cans" to apply a balanced load to the output plate. Interaction between the cans and the inside surface of the output plate generated the frictional control forces necessary to actively vary the overall torsional stiffness

of the Smart Spring as seen by the shaker. Upon receiving a positive control voltage, the stacked piezoelectric actuators elongate along the axis of the actuator unit (Fig. 6a). This causes the can "frictional surface" to move outwards against the inside surface of the output plate. The actuator assembly allows for the required axial deflections of the frictional surface while the transverse loads caused by the resulting frictional control forces are carried through the "flex rings" to the stiff outer shell of the can. Therefore, the can assembly also protected the brittle piezoelectric material from the transversal loading due to the external torque. For the monitoring of the frictional control force at each individual can, a miniature ring load cell was incorporated. The stacked piezoelectric actuators provided a blocked-force greater than 750lbf but at the relatively low voltage of 100Vac peak-to-peak.

The primary and secondary stiffness or spring arrangements are shown in Fig. 6b. In the torsional Smart Spring, both the primary and secondary torsion springs are attached to a "rigid base." The primary spring is rigidly bolted to the primary mass as seen in the left picture, and to the rigid base as indicated in the same Figure. As such, small rotations of the primary mass cause elastic twist of the torsion tube. It is important to note that the primary spring has no attachment to the secondary mass. The secondary mass is inserted around the cylindrical protrusion on the rigid base so that it rests on the "thrust bearing support." As such, there is no other cause for coupling between the primary and secondary systems besides the frictional control force. The secondary spring arrangement consists of four symmetrically cantilevered beam-type leaf springs (one was removed in Fig. 6b). The four leaf springs are bolted to the rigid base such that they are fully constrained at their root. The outer ends of the leaf springs are pinned at locations close to the outer edges. Thus, small rotation of the secondary mass causes elastic deformation in the four leaf springs.

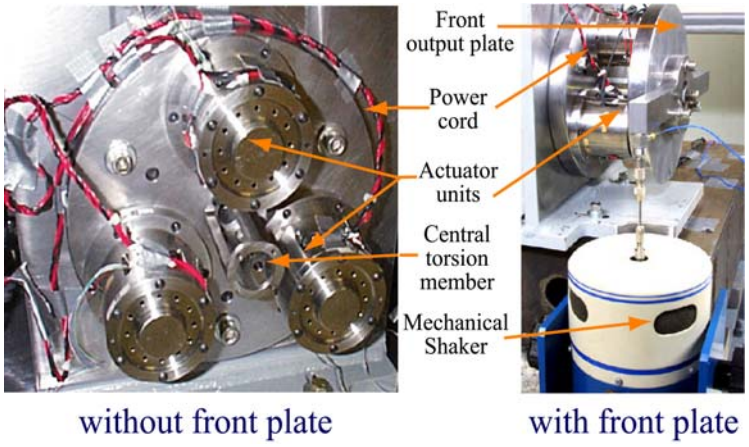

Figure 5 – Torsional Smart Spring prototype fabricated at NRCC.

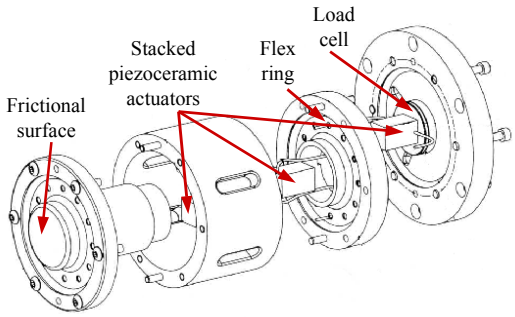

Figure 6a – Exploded view of the torsional Smart Spring prototype actuator unit (the "can assembly").

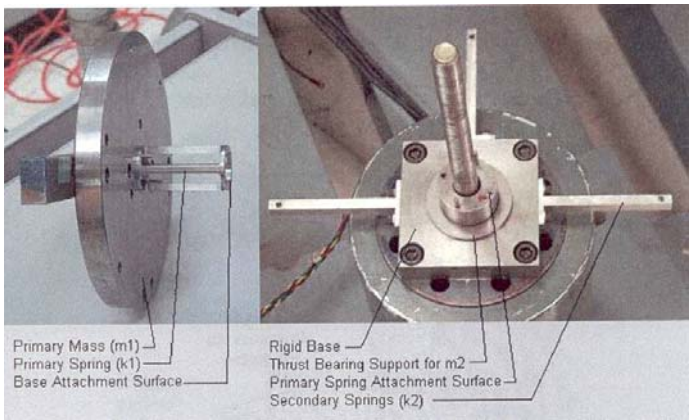

Figure 6b – Details of the torsional Smart Spring prototype device fabricated at NRCC.

The MATLAB-SIMULINK block diagram of the Smart Spring system is shown in Fig. 7. This simulation model is based on the two-degree-of-freedom conceptual drawing shown in Fig. 4 because there is no fundamental difference between the simulation models of the axial and the torsional realizations of the Smart Spring (Nitzsche and Harold, 2004). The output vector contains information about both the displacement of the controlled mass m_1 and the difference in speeds between m_2 and m_1 (the relative speed). This output value is used to compute the dynamic friction coefficient between the can "frictional surface" and the controlled mass (represented by the "output plate") using a table look-up

function. The output of the look-up table (instantaneous dynamic friction coefficient) multiplies the actuator input force to obtain the frictional control force.

A total of 11 numerical simulations are presented in Fig. 8a, corresponding to actuator input levels ranging from zero to the value of $N(t)$ sufficient to cause the primary and secondary systems to be fully coupled, at 10% increments. The mass and stiffness parameters used in the simulations were adjusted to reflect the proof-of-concept hardware and resulted in the natural frequency values of 26Hz (uncoupled system) and 35Hz (fully-coupled system). The external disturbance force, $F(t)$ was defined by a band-limited white noise. The ratio between the output displacement of the controlled mass m_1 in the frequency domain, $x_1(\omega)$ and the disturbance force, $F(\omega)$ is plotted in Fig. 8a.

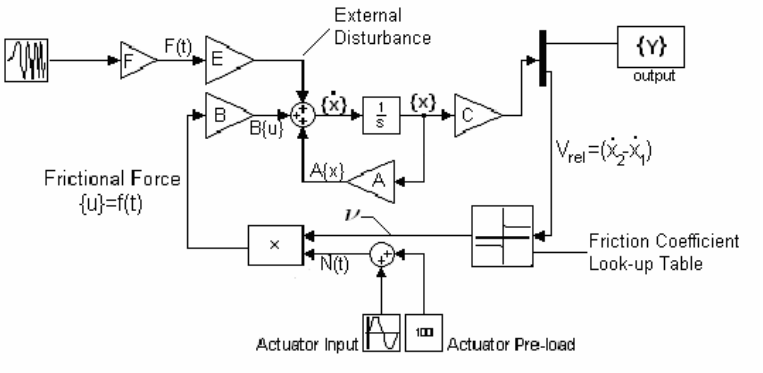

Figure 7 – Block diagram representation of the Smart Spring system.

The supporting experiment to validate the simulation model was performed at NRCC with the proof-of-concept hardware, which bears similar dynamic characteristics of the numerical model, i.e. has the same uncoupled and fully-coupled natural frequencies. The results of these experiments are presented in Fig. 8b. It can be seen that the simulation model did described the overall behavior of the actual Smart Spring device with fairly good accuracy. The main difference between the experimental and the numerical results can be seen at the low end of the frequency spectrum.

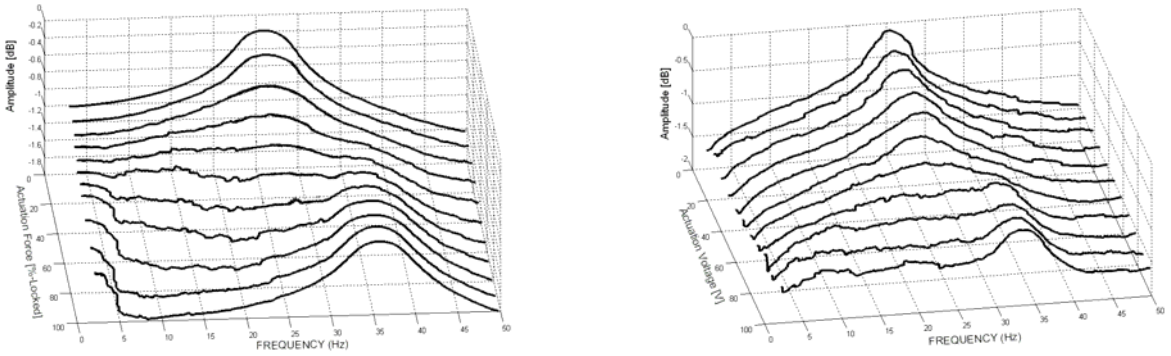

Figure 8: Smart Spring proof-of-concept hardware characteristics for different actuation levels; on the left (a) numerical simulation and on the right (b) experimental results.

Observing Figs. 8a and 8b, it can be seen that the Smart Spring system is capable of affecting both the damping levels and the natural frequency exhibited by the controlled mass. The damping in the system is reduced as the system approaches the uncoupled and fully-coupled states and sliding between the controlled mass and the secondary mass is inexistent. In addition, the system natural frequency shifts very rapidly from its uncoupled to its fully-coupled value as the actuation force approaches 50% of the latter value. This shift in natural frequency occurs in conjunction with the maximum damping level that may be obtained for the device. Hence, by actively varying its own natural frequency the Smart Spring can preferentially provide stiffness (at frequencies lower than its resonance), damping (at its resonance) or mass (at frequencies higher than its resonance) control to the hosting structure (i.e., impedance control). Furthermore, the validated simulation model suggests that the decision about the voltage applied to the piezoelectric stack is function of the relative velocity between the primary and secondary masses alone, indicating that an efficient control algorithm could be developed based on information gathered at the Smart Spring itself (Nitzsche et al, 2005).

Aeroelastic Response Attenuation using the Smart Spring

Wind tunnel tests were conducted in the low-speed facility at the Institute for Aerospace Research of the NRCC (1.9×2.7×5.2m test section) to verify the Smart Spring hardware ability to attenuate aeroelastic forced response under unsteady aerodynamic loads (Nitzsche et al, 2004). The Smart Spring was attached to one end of a 1.45m blade with a 0.3m chord in a cantilever configuration to perform impedance control of the blade torsional mode. The blade and the Smart Spring assembly were mounted on the wind tunnel force balance such that the Smart Spring device was under the floor. A 0.1m buff-body square tube was installed 1.2m upstream from the leading edge of the blade to randomly shed a stream of vortices. Accelerometers were placed on the trailing edge of the blade sections near the root and the tip to measure both the vibratory acceleration and displacement of the blade. A picture of the wind tunnel test configuration is shown in Fig. 9. At 10m/s wind speed the vortex generator produced an average buffeting torsional excitation frequency of 13.7Hz on the blade section. The amplitude as well as the frequency of the blade vibration caused by the vortex generator varied in time due to the unsteady nature of the vortex shedding phenomenon.

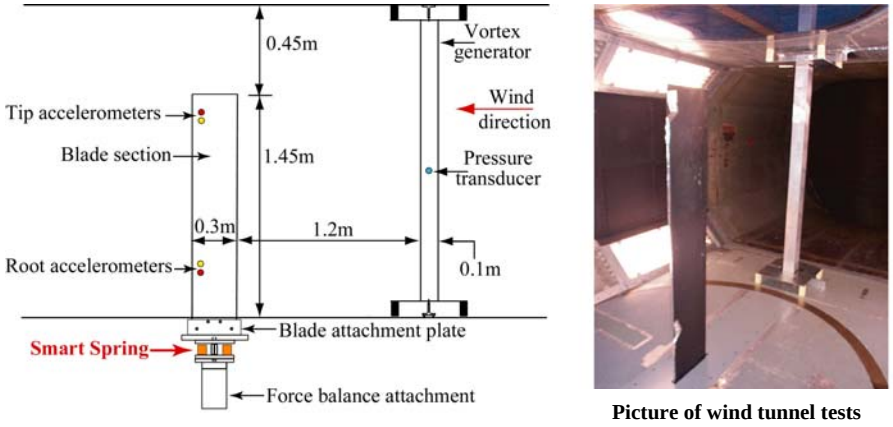

Figure 9 – Smart Spring prototype wind tunnel tests at NRCC.

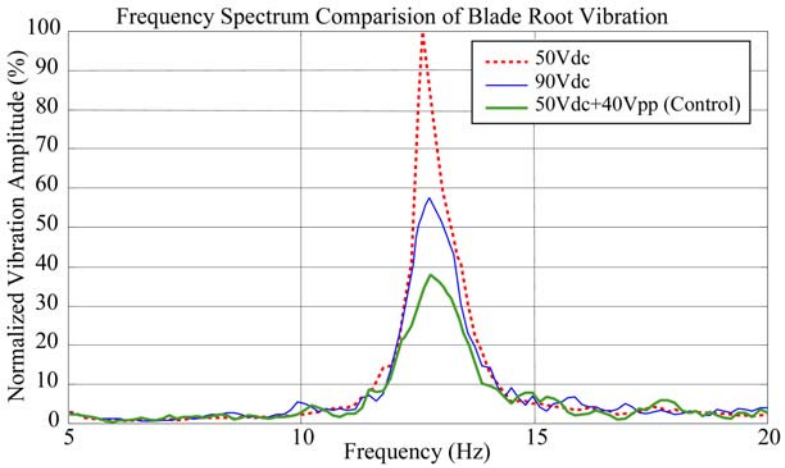

Figure 10 – Smart Spring prototype performance to attenuate the aeroelastic response in wind tunnel tests.

Frequency spectra of the blade root displacement are shown in Fig. 10. The baseline actuator operating condition was 50Vdc and this produced the highest vibratory displacement, depicted as 100%. As shown in Fig. 10, increasing the actuator voltage from 50Vdc to 90Vdc only increased the static stiffness in the Smart Spring, which in turn reduced the vibratory displacement at the blade root by 42%, indicating that this was a predominantly stiffness-controlled system. However, a higher reduction in the vibratory displacement by 62% was achieved exploiting the active impedance control characteristics of the Smart Spring. A simple open-loop control algorithm using the combined signal of 50Vdc and 40Vac peak-to-peak cycled with a 225-degree phase offset was employed (Young et al, 2004).

DIRECT-ACTIVE AND SEMI-ACTIVE HYBRID SYSTEMS

A more modern strategy to control aeroelastic phenomena using smart structures is given by the possibility of combining the direct-active and semi-active approaches in multiple-actuator hybrid systems. This could be done by employing *semi-active methods for structural control and direct-active methods for flow control*. One example is the

system that was proposed in the Smart Hybrid Active Rotor Control System (SHARCS) to attenuate vibration and noise produced by rotorcraft blades simultaneously (Nitzsche et al, 2005; Ghorashi et al, 2006).

The Smart Hybrid Active Rotor Control System (SHARCS) Project

The most advanced active control technique to attenuate noise and vibration in helicopters is called Individual Blade Control (IBC), where each blade is individually commanded independently of its azimuth angle. In the past, IBC was not fully developed due to the lack of actuators able to withstand the huge loads that characterize the helicopter rotor environment. Among the new solutions to achieve efficient IBC, the ones that involve solid-state actuators – "smart" structures are seen as the most promising. The SHARCS project is expected to demonstrate the ability of the smart structures systems, employing multiple active materials actuators, sensors and closed-loop controllers, to reduce both vibration and noise in rotorcraft. A four articulated blade rotor model, Mach and dynamically scaled, will be tested in wind tunnel in 2007 in Italy.

This international project is co-sponsored by NSERC (Natural Sciences and Engineering Research Council) and MMO (Materials Manufacturing of Ontario), an organization of the Ontario Centre of Excellence. The research also counts with the financial support of one of the major helicopter manufacturers, the consortium AgustaWestland of Italy. Carleton University coordinates the project, providing the various designs and manufacturing of the blade and the active controls subsystems. AgustaWestland provides the noise and vibration suppression requirements of a typical helicopter rotor and will supply the rotor rig for the wind tunnel tests. Other international partners include in Italy Politecnico di Milano, University of Rome ("La Sapienza") and the Third University of Rome ("Roma Tre"). The National Technical University of Athens (NTUA) of Greece completes the research group.

The SHARCS Concept

The most important components of noise and vibration produced in helicopters are originated in the main rotor from the unsteady aerodynamics that characterizes high-speed forward, maneuvering and descent flight regimes. Low-frequency vibration is mostly generated by dynamic stall in the reverse-flow region at high forward speeds, whereas high-frequency acoustic noise is produced mainly in maneuvering and descent flight regimes when the rotor blades strongly interact with the vortices shed by the tip of preceding blades, resulting in the phenomenon known as Blade Vortex Interaction (BVI). This interaction leads to an impulsive change in the blade loading that generates a pressure perturbation in the flow field above and below the rotor disk. The perturbation that propagates as a sound wave below the rotor disk reaches the ground in the form of the strong slapping noise characteristic of approaching helicopters.

The recent experiments with IBC at EUROCOPTER indicated that both noise and vibration could only be reduced marginally at the same time, although significant reductions of each individually were reported (Kloeppel and Enenkl, 2005). The explanation for this fact would be the apparent conflict of the philosophy used in the control objectives (an explanation would be that the vibration reduction mechanism involves "smoothing" the blade flight path, whereas "avoiding intersection" with the path of the impinging vortices with the objective of noise attenuation induces more vibration). The final goal of the SHARCS project is to develop a *hybrid control concept consisting of separate flow and structural control subsystems*, as sketched in Fig. 11. This approach has potential to reduce noise and vibration simultaneously in part because the problems of vibration and noise are handled by two completely independent feedback control subsystems. The Smart Spring located at the blade root can adaptively vary the impedance of the torsional mode of the blade (Active Impedance Control, AIC). It is by changing the flexural characteristics of the blade torsional mode in real time that the active control of the aeroelastic response of the entire system is achieved. Hence, the Smart Spring is the subsystem that performs *structural control*. In addition to the Smart Spring, a trailing-edge flap (Active Controlled Flap, ACF) was included in SHARCS to execute *flow control* with multiple objectives: (1) by directly alleviating the negative effects of dynamic stall on the retreating side of the rotor disc, therefore reducing at the origin the vibration excitation loads; (2) by working as a servo flap, directly exciting the first torsional mode of the blade, which in turn would control either vibration or noise depending on the implemented control law. An IBC system that provides full control authority over the first torsional mode of a rotorcraft blade will likewise be very effective to attenuate vibration and/or noise in rotorcraft. However, to achieve this property is a difficult task in practice because a blade relatively soft in torsion to allow full control authority is also prone to flutter. In SHARCS this problem can be circumvented by the Smart Spring, as it can be programmed to augment damping of the torsional mode using an energy maximum extraction algorithm (Nitzsche et al, 2005). On the other hand, BVI noise causes large fluctuations in the local lift on the advancing side of the rotor disk. Since the flap can directly change the blade lift, it has the potential to compensate for this undesired effect as well. When the lift is increasing due to a vortex passage the flap can be deflected upward to reduce lift and in the opposite sense when the lift is decreasing. These different flow control objectives can be realized by different software once the flap hardware is implemented in the blade.

The third active system in SHARCS is the blade anhedral tip angle (Active Control Tip, ACT), which can be adjusted in a quasi-steady motion to alleviate BVI at fixed rotor attitudes. This is another *flow control* device, specialized to the objective of noise attenuation at determined flight conditions such as landing. The anhedral angle affects noise by altering the trajectory of the vortices shed at the tip of the blade, increasing the "miss distance" between the blades and the stream of vortices (Aoyama et al, 1996).

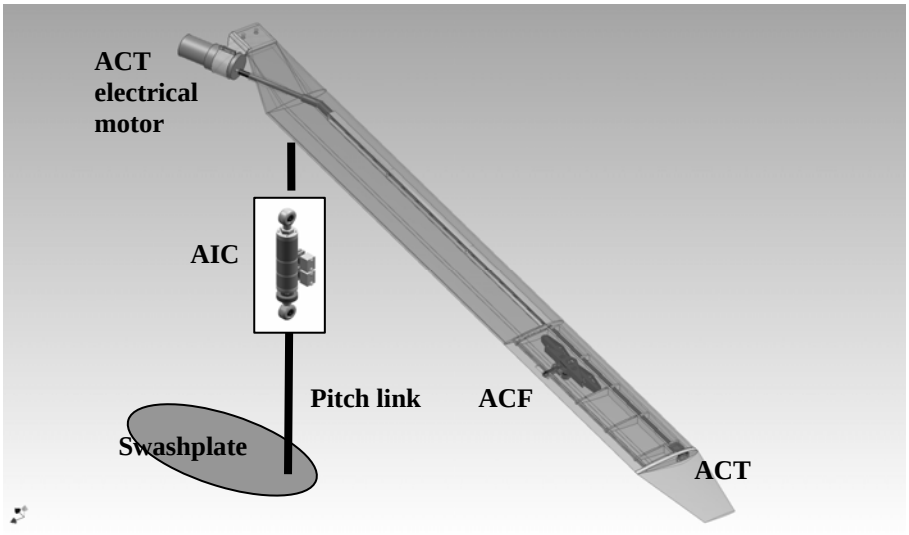

Figure 11 – The SHARCS blade "hybrid" concept incorporating direct-active (ACF and ACT) and semi-active (AIC) subsystems for rotorcraft noise and vibration control.

Realization of the Direct-active and Semi-active Subsystems of SHARCS

The **Actively Controlled Flap (ACF)** in SHARCS is *a direct-active* subsystem designed small enough to fit inside the SHARCS composite blade (1.096m length, 0.08m constant chord, NACA 0015 airfoil). The primary role of the ACF is to reduce vibrations due to dynamic stall on the retreating side of the rotor disc. The feasibility of the flap for such purpose has been demonstrated through two- and three-dimensional Computational Fluid Dynamics (CFD) simulations (Davis, Feszty and Nitzsche, 2005). It was found that the flap should be deflected with the normalized frequency with respect to the rotor fundamental frequency of 3/rev, and to deflections of about 10 degrees. For the SHARCS experimental setup, the frequency requirement was maintained, but the maximum angular deflection was limited to 4 degrees due to the lack of sufficiently powerful and at the same time compact enough actuators. Furthermore, a 4-degrees deflection is seen as enough to fulfill the servo-flap role discussed in the previous section. Hence, the APA 200M piezoelectric actuator (with a block force of 75N and a maximum deflection of 240μm) produced by Cedrat Ltd of France was selected to drive the flap actuation mechanism. The linkage lengths connecting the actuator to the flap were optimized to overcome the calculated hinge moments at the maximum angle of attack, and at the same time, maximize the flap deflection.

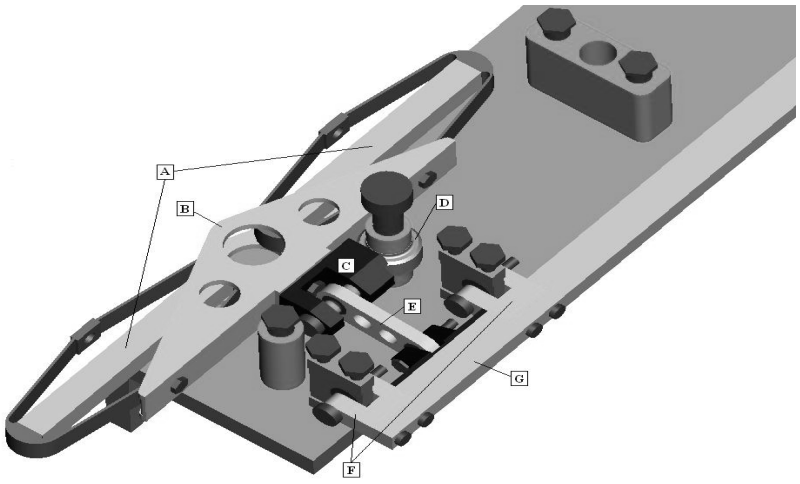

Figure 12 – SHARCS Actively Controlled Flap (ACF) direct-active subsystem: (A) piezoelectric actuators, (B) actuator pairing block, (C) slider transmission block, (D) roller, (E) control rod, (F) flap hinges, (G) flap.

Kinetically, the AFC subsystem is a slider-crank mechanism, where the linear input displacement given by the piezoelectric actuators is converted into angular displacement. The piezoelectric actuator force is used to support the aerodynamic hinge moment, the centrifugal loads of its own mass, and the friction on the mechanisms caused the rotation. The linkage includes a surface, which mates with a single roller, and provides a normal force counterbalancing the centrifugal loads. Another design consideration is the stiffness of the parts within the subsystem. For the purposes

of accurate and predictable control, it was required that each part of the linkage has minimal deflection (i.e. enough stiffness) under the expected loads. The design was heavily affected by the small scale of the blade and the huge centrifugal loads caused by the rotational speed (1550rpm to achieve the desired Mach number similarity at the blade tip). Many difficulties encountered in the design of the assembly were due to a lack of suitable miniature bearings and fasteners. For instance, ball joint bearings (which would alleviate bending reactions within the linkage) could not be used due to the width and height of the housings. Furthermore, some linkage arm lengths were smaller than the diameter of the connecting pins, requiring a more creative design of the connection. In order to minimize mass, almost all of the parts were chosen to be machined out of an aluminum alloy. However, fasteners, bearings, and the roller were made out of steel. Fig. 12 illustrates the ACF assembly prepared for the whirl tower tests that occurred at the German Aerospace Center (DLR) in Braunschweig, Germany in October 2006.

The **Actively Controlled Tip (ACT)** in SHARCS is a *direct-active* subsystem that enables the downward deflection of the blade tip up to 20 degrees to achieve noticeable effect on BVI phenomenon (Aoyama et al, 1996). The ACT is a quasi-static controller where the actuation can last for about 30s.

The first attempt to design this actuator was done using Shape Memory Alloy (SMA) wires (Lynch, Ghorashi and Nitzsche, 2005), as these materials in general produce an appropriate solution in terms of compactness and weight when the frequency response bandwidth is not an issue. A test bed was designed with the purpose to design the subsystem and its control algorithm (Fig. 13a). The experimental setup consisted of two SMA wires made of 0.015in diameter FLEXINOL 70°C that could support about 20N of tension. The wires were connected antagonistically around the top and bottom of a steel shaft. The wires pass through a pu1ley block. The shaft was supported by ball bearings that were attached to a steel plate. The rotation of the shaft was then representative of the position of the anhedral tip deflection. External loading was imposed upon the shaft by a mass and pu1ley system. The amount of tension preload in the wires was adjusted by turnbuckles. A precision potentiometer was connected to one end of the shaft, providing a measurement of its angular position. The temperature was measured with type-K thermocouples that were attached to each SMA wire and connected to signal conditioners. Data was acquired using a data acquisition board, and sent into LABVIEW for analysis and control. The control current through the SMA wires was delivered by a customized power supply, which was controlled by LABVIEW either manually by the user (open-loop) or through a computer algorithm (closed-loop). To improve the capabilities of closed-loop control, a second wire capable of providing actuation in the reverse direction was added for antagonistic control. The external loading was removed, and the SMA wires were preloaded using turnbuckles. Since the actuators worked against each other, the control algorithm was designed to carefully avoid overloading the wires. Therefore, only a single channel was actuated at any time, while the second channel either remained unaffected or was allowed to cool. Random loading input disturbances were imposed on the shaft to test the performance of the control algorithm. The magnitude of the current sent to each wire was governed by a control algorithm derived from observation and trial and error that was a function of the actual and the target shaft angles as well as the angular velocity. The closed-loop controller was able to maintain the shaft to within about ±1 degree of the target angle for both single and dual channel closed-loop feedback control (Fig. 14). The control algorithm demonstrated the feasibility of applying SMA actuator wires in an antagonistic manner for controlling the angular position of the anhedral tip flap. The performance of the controller was also robust and it was not hindered by the aforementioned random excitation of the shaft. However, the moment imposed on the hinge by the centrifugal loads caused by the ACT deflection (as high as 3.39Nm) resulted in an unfeasible number of wires necessary to overcome the external moment and the SMA concept was finally abandoned.

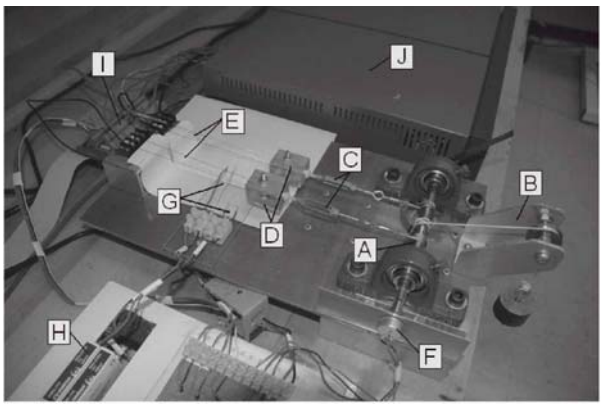

Figure 13a – SMA wires experimental setup: (A) shaft (B) mass and pulley system, (C) turnbuckles, (D) pulley blocks, (E) wires, (F) potentiometer, (G) thermocouples, (H) signal conditioners, (I) data acquisition board, (J) power supply.

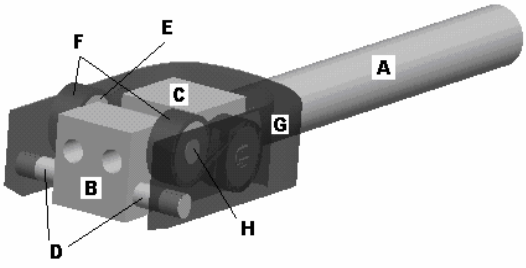

Figure 13b – SHARCS Actively Controlled Tip (ACT) direct-active actuator mechanism: (A) screw, (B) counterweight, (C) counterweight holder, (D) pin horseshoe, (E) bearing, (F) counterweight link, (G) horseshoe, (H) pin tip.

For the reason of lack of sufficient actuation provided by the SMA wires a screw-type electro-mechanical actuator design was studied next (Fig. 13b). The screw is rotated via an electric motor located at the blade root, through a light

composite torque rod spanning through the blade. The torque rod can be placed close to the airfoil leading edge. In this way, the mass of the torque rod is actually used as a replacement for portion of the required blade lead ballast. In the mechanism shown in Fig. 13b, as the screw *A* rotates, the counter weight holder *C* is moved outward, which then pivots the anhedral tip (attached to *B*) downward. The counterweight holder is made of steel so that its corresponding centrifugal force can alleviate the actuation torque, reducing the power requirement of the actuator motor. Due to size limitations, the mechanism is very small (22×16.7×9mm) with a mass of only 35g. The system demonstrated in the whirl tower tests at DLR to provide sufficient control authority, and it was then selected in the final design of the ACT.

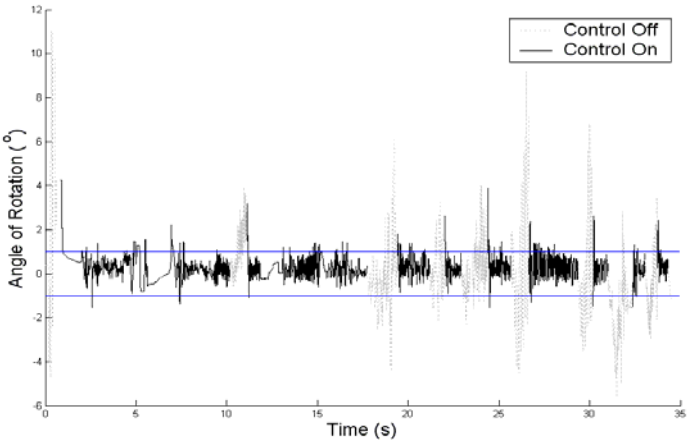

Figure 14 – SMA wires dual channel control performance to a random input disturbance.

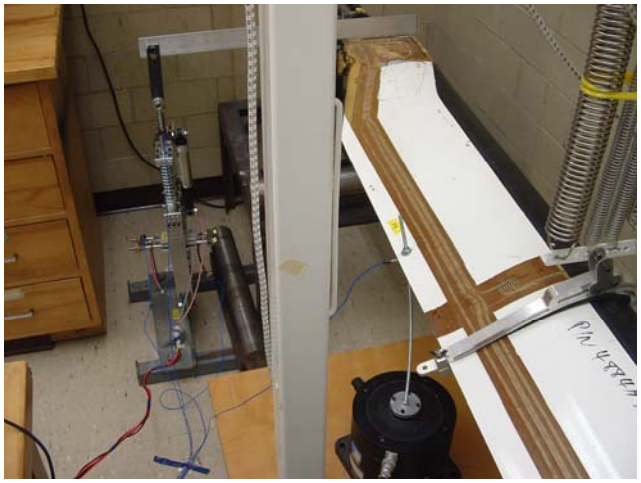

Figure 15 – The Active Impedance Control (AIC) device test bench at Carleton University.

In SHARCS the **Active Impedance Control (AIC)** device will be an improved version of the Smart Spring concept to replace the helicopter common pitch links. It will provide *semi-active* control the blade torsional mode. The main challenge was the miniaturization of the device to fit the available rotor test rig in Italy. Figure 15 illustrates the full-scale test bench that allows the testing of the AIC subsystem in the non-rotating condition that was set up at Carleton University. It incorporates a full-scale helicopter blade linked to shakers and a test model of the AIC device. The test model utilizes piezoelectric actuators supplied by Canada's Sensor Technology Ltd, and a magnetorheological controllable fluid damper from Lord Corporation, USA, which can be optionally used to adaptively tune the damping characteristics of the system. In collaboration with University of Rome "La Sapienza" the experimental system identification of the AIC device was completed (Coppotelli et al, 2006). This was the first step of the general task of developing this structural control subsystem (software and hardware). The design of the small-scale version of the AIC for the wind tunnel tests was recently completed.

CONCLUSIONS

Many concepts have been introduced to actively control aeroelastic phenomena using Smart Structures technology. These concepts can be classified into direct active and semi-active. Direct-active concepts are characterized by systems where the control action is made directly against the disturbance which is the objective of control. These systems bear in common the need of the very large control power that is still hindering practical applications of Smart Structures in

Aeroelasticity. On the other hand, semi-active concepts require much less power as the control effort is only provided to modify in real time the structural impedance properties that in turn tailor the overall aeroelastic response of the structure. Although very attractive, semi-active concepts still have limited applications. However, in an effective Smart Structure design both types of concepts should coexist in a hybrid approach where multiple aeroelastic control objectives could be addressed simultaneously by a series of cooperative subsystems specialized either for structural or flow control. It is suggested that optimized hybrid solutions will make feasible in near future the practical use of Smart Structures in the control of aeroelastic systems.

REFERENCES

Anusonti-Inthra, P., and Gandhi, F., 2000, "Helicopter Vibration Reduction through Cyclic Variations in Blade Root Stiffness," Journal of Smart Material Systems and Structures, Vol. 11, No. 2, pp. 153-166.

Aoyama, T., et al., 1996, "Calculation of rotor blade-vortex interaction noise using parallel Super Computer," Paper No. 81, Vol. 2, Proceedings of the 22nd European Rotorcraft Forum, The Royal Aeronautical Society, 16–19 September.

Coppotelli, G., et al, 2006, "SHARCS Project: Modal Parameters Identification of Smart Spring / Helicopter Blade System," Paper No. 2035, Proceedings of the 47th AIAA/ASME/ASCE/AHS/ASC Structures, Structural Dynamics and Materials Conference, Newport, RI, USA, 1–4 May.

Davis, G.L., Feszty, D. and Nitzsche, F, 2005, "Trailing edge flap flow control for the mitigation of dynamic stall effects", Paper No. 053, Proceedings of the 31st European Rotorcraft Forum, Florence, Italy, 12–14 September.

Ghorashi, M., et al, 2006,"The preliminary design of a scaled rotor blade with vibration and noise control devices," Paper No. AR08, Proceedings of the 32nd European Rotorcraft Forum, Maastricht, The Netherlands, 12–14 September.

Jaenker, J., et al, 2006,"Advanced Piezoelectric Servo-flap System for the Rotor Active Control," Paper No. AR10, Proceedings of the European Rotorcraft Forum, Maastricht, The Netherlands, 12–14 September.

Kloeppel, V. and Enenkl, B., 2005, "Rotor Blade Control by Active Helicopter Servo Flaps," Paper No. IF-158, Proceedings of the International Forum on Aeroelasticity and Structural Dynamics (IFASD 2005), Munich, Germany, 28 June – 1 July.

Lynch, B., Ghorashi, M., and Nitzsche, F., 2005, "On the Use of Shape Memory Alloy Wires for Anhedral Angle Control in Helicopter Rotor Blades," Proceedings of the 16th International Conference on Adaptive Structures Technologies, Paris, France, 9–12 October.

Nitzsche, F. Grewal, A., and Zimcik, D., 1999, "Structural component having means for cyclically varying its stiffness to control vibrations," Patent: USA (5,973,440), European Community (EP-996570-B1), Canada (2,242,214).

Nitzsche, F., 2001, "Aeroelastic Analysis of a Rotor Blade with Active Impedance Control at the Root," Canadian Aeronautics and Space Journal, Vol. 47, No. 1, pp. 7-16.

Nitzsche, F., et al, 2004, "Control Laws for an Active Tunable Vibration Absorber Designed for Aeroelastic Damping Augmentation," The Aeronautical Journal of the UK Royal Aeronautical Society, Vol. 108, No. 1079, pp. 35-42.

Nitzsche, F., and Harold, T., 2004,"Experimental System Identification of the Smart Spring Device for Semi-Active Vibration Control," Proceedings of the 15th International Conference on Adaptive Structures and Technology, Bar Harbor, ME, USA, 24–27 October.

Nitzsche, F., et al, 2005, "Development of a Maximum Energy Extraction Control for the Smart Spring," Journal of Intelligent Material Systems and Structures, Vol. 16, No. 11-12, pp. 1057-1066.

Ryall, T.G., et al, 1999, "Buffet Load Alleviation," Proceedings of the Second Australasian Congress on Applied Mechanics, Canberra, Australia, 10–12 February.

Shin, S-J, Cesnik, C.E.S., and Hall, S.R., 2005, "Closed-loop Control Test of the NASA/Army/MIT Active Twist Rotor," Journal of the American Helicopter Society, Vol. 50, No. 2, pp. 178-194.

Straub, F.K., et al, 2001,"Development of a Piezoelectric actuator for Trailing Edge Flap Control of Full Scale Rotor Blades," Journal of Smart Materials and Structures, Vol. 10, No. 1, pp. 25-34.

Young, C., et al, 2004,"Development of the Smart Spring for Active Vibration Control of Helicopter Blades," Journal of Intelligent Material Systems and Structures, Vol. 15, pp. 37-47.

Wickramasinghe, V.K., Chen, Y., and Zimcik, D., 2006, "Experimental Evaluation of a Full-Scale Advanced Hybrid Buffet Suppression System for the F/A-18 Vertical Tail," Paper No. 2136, Proceedings of the 47th AIAA/ASME/ ASCE/AHS/ASC Structures, Structural Dynamics and Materials Conference, Newport, RI, USA, 1–4 May.

Wilbur, M.L., et al, 2002, "Vibratory Loads Reduction Testing of the NASA/ARMY/MIT Active Twist Rotor," Journal of the American Helicopter Society, Vol. 47, No. 2, pp. 123-133.

RESPONSIBILITY NOTICE

The author is the only responsible for the printed material included in this paper.